SQM studied in the Field Correlator Method

F. I. M. Pereira*

Observatório Nacional, MCTI, Rua Gal. José Cristino 77, 20921-400 Rio de Janeiro RJ, Brazil
(Dated: June 9, 2022)

By using the recent nonperturbative equation of state of the quark gluon plasma derived in the formalism of the Field Correlator Method, we investigate the bulk properties of the strange quark matter in beta-equilibrium and with charge neutrality at T=p=0. The results show that the stability of strange quark matter with respect to $^{56}F_{\rm e}$ is strongly dependent on the model parameters, namely, the gluon condensate G_2 and the $q\bar{q}$ interaction potential V_1 . A remarkable result is that the width of the stability window decreases as V_1 increases, being maximum at $V_1=0$ and nearly zero at $V_1=0.5$ GeV. For V_1 in the range $0 \le V_1 \le 0.5$ GeV, all values of G_2 are lower than 0.006-0.007 GeV⁴ obtained from comparison with lattice results at T_c ($\mu=0$) ~ 170 MeV. These results do not favor the possibilities for the existence of (either nonnegative or negative) absolutely stable strange quark matter.

Keywords: Strange quark matter; Nonperturbative equation of state.

I. INTRODUCTION

Since the works of A. R. Bodmer [1] and E. Witten [2], the existence of strange quark matter (SQM) has been largely investigated. SQM is a particular form of matter comprising roughly equal amounts of u, d and s quarks. It is presumed that SQM has been produced at extreme conditions of high temperatures and densities in the beginning of the universe and/or latter at low temperatures and high densities in compact stellar interiors (e. g., neutron stars and quark stars). In this regard, it is of importance to mention the pioneer work of N. Itoh, who investigated the possibilities for the existence of hypothetical quark stars [3].

According to the Bodmer-Witten conjecture, SQM might be more stable than ordinary

^{*}Electronic address: flavio@on.br

nuclear matter. In a pioneer work, E. Farhi and R. L. Jaffe [4] investigated SQM in equilibrium with respect to weak interactions, at zero temperature and pressure, in the context of the MIT Bag Model [5]. In this model, quarks enter in the respective equation of state (EOS) as a free quark gas with a Fermi-Dirac distribution. The confinement is represented by a bag enclosing the free quarks with a constant B which gives the vacuum energy density difference between the confined and deconfined phases. Improvement of the model is obtained by the inclusion of corrections to first order in the QCD coupling constant in the $\alpha_c < 1$ (perturbative) regime (see [4] and references therein). Until now, SQM properties in dense nuclear matter and compact stars interiors have mostly been considered in the framework of the MIT Bag Model [4, 6–20]. Applications of the Nambu-Jona-Lasinio [21, 22] quantum field theoretical approach have also been done to describe quark matter properties in compact stars interiors [10, 11, 23–27]. In alternative investigations, in which quark masses are density dependent, SQM is also taken as a free Fermi gas mixture of quarks and anti-quarks |28, 29|. These approaches are used to describe u, d and s quark matter at zero and (not so high) nonzero temperatures and large density regions where the approximation of free quarks can be considered. However, this is not so at all densities and (low) temperatures. Quarks strongly interact subjected to a potential that is large when the $q\bar{q}$ distances are large. In this case, nonperturbative methods must be considered.

QCD, the fundamental theory of strong interactions, due to its nonlinearity has been taken as an inappropriate theory for the purposes of practical applications as, for instance, the calculation of an EOS to describe quark matter at all finite temperatures and densities, including nonperturbative effects of confinement. Asymptotically, the description of quark matter becomes simple, but at low temperatures and (or moderate) densities the attempts to obtain an EOS including the confinement have appeared as a difficult task to be achieved. However, since 1987, the investigations of Yu. A. Simonov [30] and H. G. Dosch [31–33] have resulted in the construction of an important method based on vacuum field correlators functions that is being continuously developed up to now.

Recently the nonperturbative EOS of quark-gluon plasma was derived in the framework of the Field Correlator Method (FCM) [34], also called Stochastic Vacuum Model. FCM (for a review see [35] and references therein) is a nonperturbative approach which naturally includes from first principles the dynamics of confinement in terms of color electric and color magnetic correlators. The parameters of the model are the gluon condensate G_2 and the

 $q\bar{q}$ interaction potential V_1 which govern the behavior of the EOS, at fixed quark masses and temperature. FCM has been used to describe the quark-gluon plasma dynamics and phase transition [36–39]. An important feature of the model is that it covers the entire phase diagram plane, from the large temperature and small density region to the small temperature and large density region. In the connection between FCM and lattice simulations, the critical temperature at $\mu_c = 0$ turns out to be $T_c \sim 170$ MeV for $G_2 \simeq 0.006 - 0.007$ GeV⁴ [36, 37].

In a previous work, the existence of stable SQM on strange star surfaces (see Sec.3.3 in [40]) was shortly considered in the FCM framework. In the present work, we perform a more detailed investigation of SQM on the same line. The system is a gas of u, d and s quarks and gluons subjected to the interaction potential V_1 . The vacuum energy density difference between confined and deconfined phases, $\Delta |\varepsilon_{vac}|$, is a nonperturbative quantity expressed in terms of G_2 . The main parameters of our calculation are $\Delta |\varepsilon_{vac}|$ (or G_2) and V_1 , and the strange quark mass m_s (assuming $m_u = m_d = 0$). We first investigate the energy per baryon, from which we obtain the stability window with respect to the $^{56}F_e$ nucleus. Strangeness, hadronic electric charge and density are also addressed.

This application of the FCM to the study of the bulk properties of SQM (not considered before) shows the role of the method to provide alternative indications for its parameters. In [40] we have shown the importance of the comparison of the FCM calculations with astrophysical observations of some strange star candidates. Similarly, in the present work, the main purpose is the relevance of the FCM predictions for the SQM properties to be compared with lattice simulations and/or the results at RHIC and LHC experiments.

This paper is organized as follows. In Sec. II we summarize the theoretical framework of the FCM and show the equations to be used in our calculation. In Sec. III we show the results and in Sec. IV we give the final remarks and conclusions.

II. BASICS EQUATIONS

In the FCM approach, the confined-deconfined phase transition is dominated by the nonperturbative correlators [35]. The dynamic of deconfinement is described by Gaussian (quadratic in $F_{\mu\nu}^a F_{\mu\nu}^a$) colorelectric and colormagnetic gauge invariant Fields Correlators $D^E(x)$, $D_1^E(x)$, $D^H(x)$, and $D_1^H(x)$. The main quantity which governs the nonperturbative dynamics of deconfinement is given by the two point functions (after a decomposition is

made)

$$g^{2} \left\langle \hat{t}r_{f}[E_{i}(x)\Phi(x,y)E_{k}(x)\Phi(y,x)] \right\rangle_{B} = \delta_{ik}[D^{E} + D_{1}^{E} + u_{4}^{2}\frac{\partial D_{1}^{E}}{\partial u_{4}^{2}}] + u_{i}u_{k}\frac{\partial D_{1}^{E}}{\partial u^{2}}$$
(1)

$$g^{2} \left\langle \hat{t}r_{f} [H_{i}(x)\Phi(x,y)H_{k}(x)\Phi(y,x)] \right\rangle_{B} = \delta_{ik} [D^{H} + D_{1}^{H} + u_{4}^{2} \frac{\partial D_{1}^{H}}{\partial u_{4}^{2}}] - u_{i}u_{k} \frac{\partial D_{1}^{H}}{\partial u^{2}}$$
(2)

where u = x - y and

$$\Phi(x,y) = P \exp\left[ig \int_{x}^{y} A_{\mu} dx^{\mu}\right] \tag{3}$$

is the parallel transporter (Schwinger line) to assure gauge invariance.

In the confined phase (below T_c), $D^E(x)$ is responsible for confinement with string tension $\sigma^E = (1/2) \int D^E(x) d^2x$. Above T_c (deconfined phase), $D^E(x)$ vanishes while $D_1^E(x)$ remains nonzero being responsible (toghether with the magnetic part due to $D^H(x)$ and $D_1^H(x)$) for nonperturbative dynamics of the deconfined phase. In lattice calculations, the nonperturbative part of $D_1^E(x)$ is parametrized in the form [35, 41]

$$D_1^E(x) = D_1^E(0)e^{-|x|/\lambda}$$
, (4)

where $\lambda = 0.34$ fm (full QCD) is the correlation length, with the normalization fixed at $T = \mu = 0$,

$$D^{E}(0) + D_{1}^{E}(0) = \frac{\pi^{2}}{18}G_{2} , \qquad (5)$$

where G_2 is the gluon condensate [42].

The generalization of the FCM at finite T and μ provides expressions for the thermodynamics quantities where the leading contribution is given by the interaction of the single quark and gluon lines with the vacuum (called single line approximation (SLA)). As in [40], from [34] and standard thermodynamical relations [43], we here explicitly rewrite in more convenient forms (for our purposes) the expressions (for one quark system, $N_f = 1$) for the pressure

$$p_q^{SLA} = \frac{1}{3} \frac{2N_c}{(2\pi)^3} \int d^3k \frac{k^2}{E} \left[f_q^{SLA}(T, J_1^E, \mu_q) + \bar{f}_q^{SLA}(T, J_1^E, \mu_q) \right] , \tag{6}$$

energy density

$$\varepsilon_q^{SLA} = \frac{2N_c}{(2\pi)^3} \int d^3k \left[E - T(T\frac{\partial J_1^E}{\partial T} + \mu_q \frac{\partial J_1^E}{\partial \mu_q}) \right] \left[f_q^{SLA}(T, J_1^E, \mu_q) + \bar{f}_q^{SLA}(T, J_1^E, \mu_q) \right] , \quad (7)$$

and include the number density of the quark system

$$n_q^{SLA} = \frac{2N_c}{(2\pi)^3} \int d^3k \left[f_q^{SLA}(T, J_1^E, \mu_q) - \bar{f}_q^{SLA}(T, J_1^E, \mu_q) \right] - T \frac{\partial J_1^E}{\partial \mu_q} \frac{2N_c}{(2\pi)^3} \int d^3k \left[f_q^{SLA}(T, J_1^E, \mu_q) + \bar{f}_q^{SLA}(T, J_1^E, \mu_q) \right],$$
 (8)

where

$$f_q^{SLA}(T, \mu_q, J_1^E) = \frac{1}{e^{\beta(E+TJ_1^E - \mu_q)} + 1}$$
 and $\bar{f}_q^{SLA}(T, \mu_q, J_1^E) = \frac{1}{e^{\beta(E+TJ_1^E + \mu_q)} + 1}$ (9)

 $(q=u,d,s), E=\sqrt{k^2+m_q^2}, \beta=1/T, \text{ and } J_1^E\equiv V_1/2T \text{ is the exponent of the Polyakov loop in the fundamental representation, where$

$$V_1 = \int_0^\beta d\tau (1 - \tau T) \int_0^\infty \xi d\xi D_1^E(\sqrt{\xi^2 + \tau^2}) . \tag{10}$$

is the large distance static qq potential [34, 35, 41].

The pressure and energy density of gluons are given by

$$p_{gl}^{SLA} = \frac{(N_c^2 - 1)}{3} \frac{2}{(2\pi)^3} \int d^3k \frac{k}{e^{\beta(k+T\tilde{J}_1^E)} - 1}$$
 (11)

and

$$\varepsilon_{gl}^{SLA} = 3 \ p_{gl} - T^2 \frac{\partial \tilde{J}_1^E}{\partial T} (N_c^2 - 1) \frac{2}{(2\pi)^3} \int d^3k \frac{1}{e^{\beta(k+T\tilde{J}_1^E)} - 1} \ , \tag{12}$$

where $\tilde{J}_1^E = \frac{9}{4}J_1^E$ is the exponent of the Polyakov loop in the adjoint representation. In Eqs.(9), (11) and (12), when $V_1 = 0$ we recover the ordinary Fermi and Bose gases. In order to give Eqs.(6)-(12) in its most general forms, it was assumed that V_1 is, in principle, a function of temperature and chemical potential. However, according to the parametrization given by Eq. (10), V_1 does not depend on the chemical potential. As pointed out in [36], the expected μ -dependence of V_1 should be weak for values of μ much smaller than the scale of vacuum fields (which is of the order of ~ 1.5 GeV) and is partially supported by the lattice simulations [44]. As in [40, 45, 46], we take V_1 independent of the chemical potential, so $\partial J_1^E/\partial \mu_q = 0$ in Eqs. (7) and (8).

In order to take into account the presence of electrons to keep the quark matter in β equilibrium and with charge neutrality, we also include the equations for the pressure, energy
density and number density of electrons given by

$$p_{\rm e} = \frac{1}{3} \frac{2}{(2\pi)^3} \int d^3k \frac{k^2}{E_{\rm e}} [f_{\rm e}(T, \mu_{\rm e}) + \bar{f}_{\rm e}(T, \mu_{\rm e})] , \qquad (13)$$

$$\varepsilon_{\rm e} = \frac{2}{(2\pi)^3} \int d^3k \ E_{\rm e}[f_{\rm e}(T, \mu_{\rm e}) + \bar{f}_{\rm e}(T, \mu_{\rm e})] \ ,$$
 (14)

$$n_{\rm e} = \frac{2}{(2\pi)^3} \int d^3k [f_{\rm e}(T, \mu_{\rm e}) - \bar{f}_{\rm e}(T, \mu_{\rm e})] ,$$
 (15)

where

$$f_{\rm e}(T,\mu_{\rm e}) = \frac{1}{{\rm e}^{\beta(E_{\rm e}-\mu_{\rm e})}+1} \quad , \quad \bar{f}_{\rm e}(T,\mu_{\rm e}) = \frac{1}{{\rm e}^{\beta(E_{\rm e}+\mu_{\rm e})}+1}$$
 (16)

and $E_{\rm e} = \sqrt{k_{\rm e}^2 + m_{\rm e}^2}$.

The composition of SQM is maintained in β -equilibrium with respect to weak interactions and in electric charge neutrality. The weak interactions reactions are given by

$$d \to u + e + \bar{\nu}_e \tag{17}$$

and

$$s \to u + e + \bar{\nu}_e$$
 (18)

As pointed out in [4], the neutrino gas is so dilute that it play no role in the dynamics of the system. So, by neglecting the neutrino chemical potential, the chemical equilibrium equations are given by

$$\mu_d = \mu_u + \mu_e \tag{19}$$

and

$$\mu_s = \mu_d \ . \tag{20}$$

The overall charge neutrality requires that

$$\frac{1}{3}(2n_u^{SLA} - n_d^{SLA} - n_s^{SLA}) - n_e = 0.$$
 (21)

By numerically solving Eqs. (19)-(21), for each value of the input total density

$$n = n_u^{SLA} + n_d^{SLA} + n_s^{SLA} + n_e , (22)$$

the unknown chemical potentials $\mu_{\rm u}$, $\mu_{\rm d}$, $\mu_{\rm s}$ and $\mu_{\rm e}$ are determined for fixed values of T, G_2 and V_1 . However, our calculation here is slightly different from that in [40], as explained below.

The total pressure and energy density of the quark-gluon system, including electrons are given by

$$p = p_{gl}^{SLA} + \sum_{q=u,d,s} p_q^{SLA} - \Delta |\varepsilon_{vac}| + p_e , \qquad (23)$$

$$\varepsilon = \varepsilon_{gl}^{SLA} + \sum_{q=u,d,s} \varepsilon_q^{SLA} + \Delta |\varepsilon_{vac}| + \varepsilon_e , \qquad (24)$$

where

$$\Delta|\varepsilon_{vac}| = \frac{11 - \frac{2}{3}N_f}{32}\Delta G_2 , \qquad (25)$$

is the vacuum energy density defference between confined and deconfined phases in terms of the respective difference between the values of the gluon condensate, $\Delta G_2 = G_2(T < T_c) - G_2(T > T_c) \simeq \frac{1}{2}G_2$ [36, 37], and N_f is the number of flavors.

We follow the same line of [4] to investigate the behavior of the SQM at zero temperature¹ and total pressure by solving the above equations for constant values of the energy per baryon, $E/A = \varepsilon/n_A$, where $n_A = (n_u + n_d + n_s)/3$ is the baryon number density. We perform our calculation in the $m_u = m_d = 0$ approximation² (in Sec. III, larger values of m_u and m_d are speculated in order to look for strangeness excess and negative electric charge possibilities). By using the constant E/A constraint in the above equations, m_s and $\Delta|\varepsilon_{vac}|$ (or G_2) are determined for fixed values of V_1 in the range $0 \le V_1 \le 0.5$ GeV (where $V_1 = 0.5$ GeV is the value of V_1 at $T = T_c$ obtained from lattice investigations [47]). As in [40, 45, 46], our calculation here is made for V_1 constant, so $T^2 \partial J_1^E/\partial T = -V_1/2$ in Eq. (7).

A. Quark matter at T = 0 and constant V_1 .

For pedagogical purposes, we show the previous equations for the quark system at zero temperature and constant V_1 for the general case of nonzero quark masses. Zero temperature implies that

$$f_q^{SLA}(T, \mu_q, J_1^E) \xrightarrow[T \to 0]{} \Theta(\mu_q - E - TJ_1^E)$$
 (26)

and Eqs.(6)-(8) lead to

$$p_q^{SLA} = \frac{N_c}{3\pi^2} \left\{ \frac{k_q^3}{4} \sqrt{k_q^2 + m_q^2} - \frac{3}{8} m_q^2 \left[k_q \sqrt{k_q^2 + m_q^2} - m_q^2 \ln \left(\frac{k_q + \sqrt{k_q^2 + m_q^2}}{m_q} \right) \right] \right\}, \quad (27)$$

¹ In reality, we take T = 0.001 GeV in Eqs. (6-15) which is a good approximation or, alternatively, by using Eqs. (27) - (29).

² For our purposes here, it is irrelevant if electrons are assumed massless or not.

$$\varepsilon_q^{SLA} = \frac{N_c}{\pi^2} \left\{ \frac{k_q^3}{4} \sqrt{k_q^2 + m_q^2} + \frac{m_q^2}{8} \left[k_q \sqrt{k_q^2 + m_q^2} - m_q^2 \ln \left(\frac{k_q + \sqrt{k_q^2 + m_q^2}}{m_q} \right) \right] + \frac{V_1}{2} \frac{k_q^3}{3} \right\}$$
(28)

and

$$n_q^{SLA} = \frac{N_c}{\pi^2} \, \frac{k_q^3}{3} \,, \tag{29}$$

where

$$k_q = \sqrt{(\mu_q - V_1/2)^2 - m_q^2}, \quad (q = u, d, s).$$
 (30)

When $V_1 = 0$, the ordinary Fermi momentum k_F is recovered.

1. Zero mass approximation

In order to better understand the role of G_2 and V_1 in the study of stability of quark matter, it is instructive to apply the above equations to quark matter at zero temperature and pressure, assuming that all quark species are massless particles. This simple case serve to help us to understand the behavior of the constant E/A curves in Fig. 1, as well as the shrinking of the stability window in panel (a) of Fig. 3, at $m_s = 0$. For massless quarks, Eqs.(27)-(29) (with $N_c = 3$), by using Eq.(30), are reduced to

$$p_q^{SLA} = \frac{1}{4\pi^2} \left(\mu_q - \frac{V_1}{2} \right)^4, \tag{31}$$

$$\varepsilon_q^{SLA} = \frac{1}{\pi^2} \left\{ \frac{3}{4} \left(\mu_q - \frac{V_1}{2} \right)^4 + \frac{V_1}{2} \left(\mu_q - \frac{V_1}{2} \right)^3 \right\}$$
 (32)

and

$$n_q^{SLA} = \frac{1}{\pi^2} \left(\mu_q - \frac{V_1}{2} \right)^3. \tag{33}$$

At total zero pressure, the sum of the quark pressures is balanced by the vacuum energy density,

$$\sum_{q} \frac{1}{4\pi^2} \left(\mu_q - \frac{V_1}{2} \right)^4 - \Delta |\varepsilon_{vac}| = 0 , \qquad (34)$$

and the energy density is

$$\varepsilon = \sum_{q} \varepsilon_{q} + \Delta |\varepsilon_{vac}|$$

$$= 3 \sum_{q} p_{q} + \frac{V_{1}}{2\pi^{2}} \sum_{q} \left(\mu_{q} - \frac{V_{1}}{2}\right)^{3} + \Delta |\varepsilon_{vac}|$$

$$= \frac{3}{2} V_{1} n_{A} + 4 \Delta |\varepsilon_{vac}|$$
(35)

where (here, in this section) the baryon number density is $n_A = (n_u + n_d + n_s)/3$ for SQM and $n_A = (n_u + n_d)/3$ for nonstrange quark matter. Notice the presence of the additional term $(3/2)V_1n_A$ with respect to the corresponding expressions in the MIT Bag Model [9]. Also noticed is that the sum of the quark pressures and energy densities are given in terms of $\Delta |\varepsilon_{vac}|$ (or G_2) and V_1 (differently from the MIT Bag Model where they are given solely in terms of the bag constant B). Now, let us particularize the above equations for two and three flavor quark matter.

Two flavor

For a gas of u and d quarks, charge neutrality (neglecting the not important cotribution of electrons as in [9]) requires that $n_d^{SLA} = 2 n_u^{SLA}$, from which it follows that $(\mu_d - V_1/2) = 2^{1/3}(\mu_u - V_1/2)$. The two-flavor vacuum energy density (for $N_f = 2$ in Eq.(25)) is $\Delta |\varepsilon_{vac}|_{ud} = (29/192) G_2$. Thus, the energy per baryon of the ud system is

$$\left(\frac{E}{A}\right)_{ud} = (1 + 2^{4/3})^{3/4} (4\pi^2)^{1/4} (\Delta |\varepsilon_{vac}|_{ud})^{1/4} + \frac{3}{2} V_1$$

$$= 6.441 (\Delta |\varepsilon_{vac}|_{ud})^{1/4} + \frac{3}{2} V_1$$

$$= 4.016 G_2^{1/4} + \frac{3}{2} V_1. \tag{36}$$

Three flavor

The three flavor quark system (SQM) is naturally charge neutral, with $n_u^{SLA} = n_d^{SLA} = n_s^{SLA}$, $\mu_u = \mu_d = \mu_s = \mu$, and $n_e = \mu_e = 0$. The vacuum energy density (for $N_f = 3$) is $\Delta |\varepsilon_{vac}| = (9/64)~G_2$, and the energy per baryon becomes (using the previous notation for the SQM system, without subscripts)

$$\left(\frac{E}{A}\right) = 3^{3/4} (4\pi^2)^{1/4} (\Delta |\varepsilon_{vac}|)^{1/4} + \frac{3}{2} V_1$$

$$= 5.714 (\Delta |\varepsilon_{vac}|)^{1/4} + \frac{3}{2} V_1$$

$$= 3.499 G_2^{1/4} + \frac{3}{2} V_1. \tag{37}$$

In Eqs.(36) and (37), for fixed E/A, the increase of $V_1(G_2)$ is compensated by the corresponding decrease of $G_2(V_1)$. As shown below in Fig. 1, (at $m_s = 0$ and a given E/A) the maximum value of G_2 is obtained for $V_1 = 0$.

The energy per baryon of ${}^{56}F_{\rm e}$ is 930.4 MeV, so in this simple analysis the stability of SQM relative to iron corresponds to $G_2 < (0.266 - 0.428V_1)^4$. As a result, we obtain $G_2 < 0.005 \text{ GeV}^4$ for $V_1 = 0$, $G_2 < 0.002 \text{ GeV}^4$ for $V_1 = 0.1 \text{ GeV}$, and so on, until a very small value of G_2 ($\lesssim 10^{-5} \text{ GeV}^4$) for $V_1 = 0.5 \text{ GeV}$. This behavior explains the shrinking of the stability window at $m_s = 0$ shown in panel (a) of Fig.3.

Finally, from Eqs. (36) and (37) we obtain

$$\frac{(E/A)}{(E/A)_{ud}} = \frac{3^{3/4} (4\pi^2)^{1/4} (\Delta |\varepsilon_{vac}|)^{1/4} + 1.5 V_1}{(1 + 2^{4/3})^{3/4} (4\pi^2)^{1/4} (\Delta |\varepsilon_{vac}|_{ud})^{1/4} + 1.5 V_1}$$

$$= \frac{5.714 (\Delta |\varepsilon_{vac}|)^{1/4} + 1.5 V_1}{6.441 (\Delta |\varepsilon_{vac}|_{ud})^{1/4} + 1.5 V_1}$$

$$= \frac{3.499 G_2^{1/4} + 1.5 V_1}{4.016 G_2^{1/4} + 1.5 V_1}.$$
(38)

It is evident that $(E/A) < (E/A)_{ud}$ (for the same values of G_2 and V_1 in SQM and ud systems). From the last line of Eq.(38) it follows that $(E/A)/(E/A)_{ud} = 0.87$ for $V_1 = 0$. On the other hand, for the MIT Bag Model, with the correspondences $\Delta |\varepsilon_{vac}| = \Delta |\varepsilon_{vac}|_{ud} \equiv B$ and $V_1 = 0$, we obtain $(E/A)/(E/A)_{ud} = 0.89$ as in [9].

III. RESULTS

We are concerned with the bulk properties of SQM and concentrate ourselves to investigate the stability with respect to the $^{56}F_{\rm e}$ nucleus. In our investigation, m_s enters as input parameter and $\Delta|\varepsilon_{vac}|$ (or G_2) is determined for fixed values of E/A and V_1 . By this way, as in [40], but with a different logic, we obtain a scenario for the model parameters, independently of what the results of lattice calculation may be. We discuss the relations between the parameter values required for the SQM stability and the values obtained by comparison with lattice predictions in [36, 37].

In Fig. 1, the constant E/A contours give m_s vs $\Delta |\varepsilon_{vac}|$ (for the purpose of comparison with MIT Bag Model results in [4, 8, 9]) for different values of V_1 . In order to understand the role the gluon condensate, we use the relation between $\Delta |\varepsilon_{vac}|$ and G_2 , given by Eq. (25), to plot m_s vs G_2 for the same values of V_1 . The contours are very sensitive to the values of V_1 ,

being shifted towards lower values of $\Delta|\varepsilon_{\rm vac}|$ and/or G_2 as shown for $V_1=0$ (panels (a) and (b)) and $V_1=0.01$ GeV (panels (c) and (d)). To the right of the E/A=0.93 GeV contour (in reality, 930.4 MeV corresponding to the energy per nucleon of $^{56}F_{\rm e}$), SQM is unstable with respect to the iron nuclei. The vertical line at the left of each panel is the limit of $\Delta|\varepsilon_{\rm vac}|$ and/or G_2 when m_s becomes large, so the strangeness per baryon goes to zero (see panel (a) in Fig. 2). In this case, there is no distinction between strange and non-strange quark matter. Contours with E/A < 930.4 MeV terminate at the crossing with the vertical line of $^{56}F_{\rm e}$. For $V_1=0$, the results shown in panel (a) are numerically equivalent to the ones found in the case of the MIT Bag Model. However, we remark that in the FCM the vacuum energy difference $\Delta|\varepsilon_{\rm vac}|$ is essentially a nonperturbative quantity given in terms of the gluon condensate. Also shown is the E/A=0.939 GeV contour corresponding to the nucleon mass.

Stability window of the SQM is the region of allowed values of m_s and $\Delta|\varepsilon_{\rm vac}|$ (or G_2) where the energy per particle is lower than the one of $^{56}F_{\rm e}$ (bounded by the E/A=0.93 GeV contour and the respective vertical line). In the FCM, the stability of SQM depends on the values of V_1 and/or G_2 . For a given value of E/A, the higher V_1 , the lower G_2 (cf. Eq.(37) for the case $m_s=0$). Moreover, even for $V_1=0$ (for which the contours present the maximum G_2 at $m_s=0$), the values of G_2 within the stability window are lower than $0.006-0.007~{\rm GeV}^4$ obtained from lattice data on the critical temperature [36, 37]. The possibility of the SQM be more bound than $^{56}F_{\rm e}$ is realized only for $G_2<0.005~{\rm GeV}^4$. This has also been the case for $m_u=5~{\rm MeV}$, $m_d=7~{\rm MeV}$ and $m_s=150~{\rm MeV}$ for which we have shown that $G_2<0.0041~{\rm GeV}^4$ for the existence of stable SQM in strange star surfaces [40]. Even if we take stability with respect to the nucleon mass ($E/A=0.939~{\rm GeV}$), instead of $^{56}F_{\rm e}$, the values of G_2 remain lower than the one in [36, 37].

Fig. 2 shows for the given value of E/A (the same as in [4]) the strangeness per baryon (defined as in [4]) in panel (a) as function of m_s for some values V_1 . The strangeness per baryon is always lower then unity, going to zero at $m_s \sim 0.3$ GeV (however, strangeness excess might be possible for nonzero m_u and/or m_d as shown in panel (a) of Fig. 5). For the same values of V_1 , panel (b) shows the decrease of the baryon number density from its maximum at $m_s = 0$ until a constant value around $m_s \sim 0.3$ GeV. We must be aware that for larger values of V_1 and at some value of m_s , the baryon number density n_A might becomes lower than a critical value (if it exists) at which the phase transition takes place.

However, the determination of such a critical value is not the scope of the present work.

We have also calculated the hadronic electric charge per baryon,

$$\frac{Z}{A} = \frac{2n_u - n_d - n_s}{n_u + n_d + n_s} = \pm \frac{n_e}{n_A} \,, \tag{39}$$

shown in panel (c). For $m_s = 0$ the equilibrium configuration is given by an equal number of u, d and s quarks ($n_u = n_d = n_s$ and $n_e = 0$) with zero electric charge. When m_s and/or V_1 grow, the system develops a positive hadronic electric charge. For large m_s , the hadronic electric charge per baryon saturates at a constant value which also depends on V_1 (cf. panel (b) of Fig. 4). For $V_1 = 0$, this saturation point is ~ 0.0056 at $m_s \sim 0.3$ GeV as in [4].

Given that all E/A < 0.93 GeV contours are within the stability window, it is instructive to consider some features of SQM at E/A = 0.93 GeV of $^{56}F_{\rm e}$. In panel (a) of Fig. 3 we show that the overall effect of the confining forces is to shift the stability windows towards lower values of G_2 for increasing values of V_1 . The windows not only narrow as m_s grows at a fixed V_1 , but they also narrow as V_1 grows at the same value of m_s . In particular, for $V_1 = 0.5$ GeV the vertical line is located at a negligible value of G_2 and the stability window width is very small (not visible in the scale of the figure). From the locations (at fixed values of V_1) of the constant E/A contours and the respective vertical lines on the horizontal axis at $m_s = 0$, where each window presents its maximum width, we construct two plots V_1 vs G_2 as shown in panel (b). The region between the dashed and solid curves illustrates the decrease of the stability window width with V_1 . In panel (c), we show the baryon number density for $0 \le V_1 \le 0.5$ GeV. For $V_1 = 0.5$ GeV, it is nearly zero. So, as we have observed above, due to the decreasing of n_A it might happens that a quark-hadron phase transition occurs at some value of V_1 and m_s .

Fig. 4 shows the strangeness per baryon (in panel (a)) and the hadronic electric charge per baryon (in panel (b)), at the energy per baryon of $^{56}F_{\rm e}$, as function of m_s for $V_1=0$ and $V_1=0.5$ GeV. For all values of V_1 in the region $0 \le V_1 \le 0.5$ GeV and m_s in the region $0 \le m_s \lesssim 0.35$ GeV, the strangeness per baryon is always less than unity. Depending on the values of V_1 , the saturation of the hadronic electric charge per baryon is between 0.0056 for $V_1=0$ and ~ 0.006 for $V_1=0.5$ GeV (this variation is not visible in panel (c) of Fig. 2 because of the low values of V_1).

Let us now consider the question of the strangeness excess. We have performed our calculation assuming that $m_u = m_d = 0$. However, for nonzero m_u and/or m_d , strangeness

excess can be obtained which is more sensitive to m_d than it is to m_u . For the usual values of u and d quark masses, $m_u = 5$ MeV and $m_d = 7$ MeV, the strangeness excess is less than 1%, but it can be larger for larger m_u and m_d . As an ilustrative example, we have (speculatively) extrapolated m_u and m_d beyond its usual values in order to obtain a strangeness excess around 9-14 % as shown in panel (a) of Fig. 5, for the given quark masses, V_1 and E/A. Generally speaking, this excess only occurs for low values of m_s ($\lesssim 0.02$ GeV) and large values of V_1 which, in turn, correspond to very small values of G_2 ($\sim 10^{-6}$ GeV⁴) (the increase of u and d quark masses also shifts the E/A contours towards lower values of G_2).

Correspondingly, we also speculate the possibility of negative hadronic electric charge. The change of the hadronic electric charge is more sensitive to m_u and m_s than it is to m_d . For large values of V_1 , it can happen that strange quarks are more abundant than the massless u and d quarks in the region of small values of m_s . So, negative hadronic electric charge appears to be allowed for large values of V_1 , m_u and m_d (as for the case of strangeness excess), but for small m_s , as shown in panel (b). In this case, instead of electrons, a sea of positrons neutralizes the negative hadronic electric charge. We also remark that, at the same values of V_1 , m_u and m_d , larger values of S/A and lower (negative) Z/A are allowed for E/A < 0.899 GeV and m_s in the region $0 \le m_s \lesssim 0.02$ GeV.

Summarizing the above results, strangeness excess and negative hadronic electric charge per baryon are realized only for large values of m_u and/or m_d and V_1 (say, $V_1 \gtrsim 0.3$ GeV), but for values of G_2 much lower than the one in [36, 37]. For $m_u = m_d = 0$ as well as for the usual $m_u = 5$ MeV and $m_d = 7$ MeV, we observe that the values of the model parameters obtained in the present paper do not favor the existence of neither nonnegative nor negative SQM with energy per baryon lower than the one of the $^{56}F_e$ nucleus.

IV. FINAL REMARKS AND CONCLUSIONS

In this work we have investigated the bulk properties of SQM by using the quark-gluon plasma EOS derived in the FCM nonperturbative approach [34]. The important parameters of the model are the gluon condensate G_2 (which enters the EOS through the vacuum energy difference $\Delta |\varepsilon_{\text{vac}}|$ between confined and deconfined phases) and the large distance $q\bar{q}$ interaction potential V_1 . The results have shown that confinement plays an important role

for the stability of SQM.

We have performed the calculation in the $m_u = m_d = 0$ approximation and assumed SQM in β -equilibrium and charge neutrality, at zero temperature and pressure. We have been mainly concerned with the absolute stability of SQM with respect to $^{56}F_e$ nucleus. In order to look for stability windows of SQM, we have started our investigation by drawing contours of constant energy per baryon, E/A, in the m_s vs $\Delta |\varepsilon_{\text{vac}}|$ (and/or m_s vs G_2) plane for fixed values of V_1 . Strangeness and hadronic electric charge have also been considered. Our study revealed remarkable features which we summarize as follows.

The general trend is that the SQM stability is very sensitive to the values of the model parameters responsible by the confining forces. A remarkable aspect is that the behavior of the stability window strongly depends on the values of V_1 . For increasing values of this parameter, the constant E/A contours and also the respective stability windows as a whole are shifted towards lower and lower values of $\Delta|\varepsilon_{\rm vac}|$ (and/or G_2) until to ~ 0 at $V_1 = 0.5$ GeV. Moreover, the width of the stability windows diminish when V_1 becomes larger. At $m_s = 0$, it has the maximum width between $G_2 = 0.003$ GeV⁴ and $G_2 = 0.005$ GeV⁴ for $V_1 = 0$ and a nearly zero width at $G_2 \sim 0$ for $V_1 = 0.5$ GeV. This amounts to say that absolutely stable SQM would exists, in principle, for $0 \leq V_1 \leq 0.5$ GeV (although somewhat problematic at $V_1 = 0.5$ GeV due to the smallness of the corresponding value of G_2). However, a striking point is that the values of G_2 are lower than the one in the range 0.006 - 0.007 GeV⁴ obtained from comparison with the lattice data at the critical temperature [36, 37]. This point puts a severe restriction for the existence of absolutely stable SQM with respect to $^{56}F_e$.

We have also calculated the strangeness per baryon and the hadronic electric charge per baryon. As m_s grows, the strangeness per baryon decreases from S/A = 1 at $m_s = 0$ to S/A = 0 for some value of m_s which depends on E/A and V_1 . Correspondingly, the hadronic electric charge per baryon is always nonnegative, rising from Z/A = 0 up to a constant value which depends on the value of V_1 . Another remarkable feature (in the $m_u = m_d = 0$ approximation) is that $S/A \leq 1$ and $Z/A \geq 0$ for all values of m_s within the stability window.

In the attempt to find strangeness excess and negative hadronic electric charge, we have observed that S/A > 1 and Z/A < 0 appear to be allowed only for very large values of m_u and/or m_d (beyond the usual ones), but for small m_s ($\lesssim 0.02$ GeV) and large V_1 (say,

between 0.3 GeV and 0.5 GeV). However, the corresponding values of G_2 remain lower than the one in [36, 37], as in the case of $m_u = m_d = 0$.

From the above, in the context of the FCM approach, it appears that the values of the model parameters obtained in our investigation do not favor the existence of absolutely stable SQM. Of course the above results depend on the constant V_1 assumption, in the present work.

Taking into account the importance of experiments at RHIC and LHC, it is instructive at this point to consider finite temperature effects on the SQM properties. In order to check the influence of nonzero temperatures on the SQM stability at zero pressure, we have applied the same procedure employed for the T=0 case to study the behavior of the stability window shown in Fig. 3, but for $T \neq 0$. We have taken several values of T up to 30 MeV for constant V_1 and for $V_1(T)$ parametrized in [37] for $T \geq T_c$ as

$$V_1(T) = \frac{0.175 \text{ GeV}}{1.35 T/T_c - 1}, \quad V_1(T_c) = 0.5 \text{ GeV},$$
 (40)

for $T = T_c$, $2T_c$, $3T_c$ and some arbitrary values of T_c along the phase diagram transition curve. In both cases, the results are qualitatively analogous to those in Fig. 1 of [8] and Fig. 3 of [29]. However, $V_1(T)$ is decreasing with the growth of T, so the shift of the stability window towards lower values of G_2 takes place as $T \to T_c$. For $V_1(T = T_c)$ the result is the same as for constant $V_1 = 0.5$ GeV at T = 0 shown in panel (a) of Fig. 3.

Generally speaking, our results appear to be consistent with the fact that absolutely stable SQM has not been observed up to the present. The experiment with STAR at RHIC has not confirmed the existence of SQM nor proved that it does not exist [48–50]. The low values of G_2 with respect to the ones in [36, 37] would provide a possible explanation for the absence of absolutely stable SQM signature. However, before any conclusion towards the nonexistence of absolutely stable SQM, we must have in mind that our theoretical results should be a consequence of the approximations contained in the development of the FCM nonperturbative EOS. FCM is a robust theoretical approach where the dynamics of confinement is one of the most important aspects of the model. Therefore, we must be aware that the FCM nonperturbative EOS is presently developed in the so called Single Line Approximation, where the confinement dynamics include only single quarks and gluons interactions with the vacuum [34].

On the other hand, in our calculations, V_1 and G_2 were taken as μ -independent pa-

rameters. As pointed out in [45, 46], the μ -independence of V_1 should be a questionable assumption. Also, in the large density domain, important effects should be related to a possible density dependence of G_2 [51]. In our opinion, these aspects are very interesting possibilities to be considered. However, this does not have been the scope of the present work.

ACKNOWLEDGMENTS

This work was done with the support provided by the Ministério da Ciência , Tecnologia e Inovação (MCTI).

- [1] A. R. Bodmer, Phys. Rev. D4 (1971) 1601.
- [2] E. Witten, Phys. Rev. D30 (1984) 272.
- [3] N. Itoh, Prog. Theor. Phys. 44 (1970) 291.
- [4] E. Farhi, R. L. Jaffe, Phys. Rev. D30 (1984) 2379.
- [5] A. Chodos, R. L. Jaffe, K. Johnson, C. B. Thorne, V. F. Weisskopf, Phys. Rev. D9 (1961) 3471.
- [6] P. Haensel, J. L. Zdunik, R. Schaeffer, Astron. Astrophys. 160 (1986) 121.
- [7] C. Alcok, E. Farhi, A. Olinto, Astrophys. J. 310 (1986) 261.
- [8] Ch. Kettner, F. Weber, M. K. Weigel, N. K. Glendenning, Phys. Rev. D51 (1995) 1440.
- [9] J. Madsen, arXiv:astro-ph/9809032.
- [10] D. P. Menezes, C. Providência, Phys. Rev. C68 (2003) 035804.
- [11] D. P. Menezes, C. Providência, Braz. J. Phys. 34 (2004) 724.
- [12] K.Kohri, K. Iida, Sato, K., Prog. Theor. Phys. Suppl. 151 (2003) 181; arXiv:astro-ph/0210259.
- [13] W. M. Alberico, A. Drago, C. Ratti, Nucl. Phys. A706 (2002) 143.
- [14] G. F. Burgio, M. Baldo, P. K. Sahn, A. B. Santra, H. -J. Schulze, Phys. Lett. B526 (2002) 19.
- [15] G. F. Burgio, M. Baldo, P. K. Sahn, H. -J. Schulze, Phys. Rev. C66 (2002) 025802.
- [16] C. Maieron, M. Baldo, G. F. Burgio, H. -J. Schulze, Phys. Rev. D70 (2004) 043010.
- [17] T. Boeckel, M. Hempel, I. Sagert, G. Pagliara, B. Sa'd, J. Schaffner-Bielich, J. Phys. G: Nucl. Part. Phys. 37 (2010) 094005.
- [18] Irina Sagert, T. Fischer, M. Hempel, G. Pagliara, J. Schaffner-Bielich, F.-K. Thielemann, M. Liebendörfer, J. Phys. G: Nucl. Part. Phys. 37 (2010) 094064.

- [19] Giuseppe Pagliara, Matthias Hempel, Jürgen Schaffner-Bielich, J. Phys. G: Nucl. Part. Phys. 37 (2010) 094065.
- [20] B. W. Mintz, E. S. Fraga, J. Schaffner-Bielich, G. Pagliara, J. Phys. G: Nucl. Part. Phys. 37 (2010) 094066.
- [21] Y. Nambu, G. Jona-Lasinio, Phys. Rev. 122 (1961) 345.
- [22] Y. Nambu, G. Jona-Lasinio, Phys. Rev. 124 (1961) 246.
- [23] M. Baldo, M. Buballa, G. F. Burgio, F. Neumann, M. Oertel, H.-J. Schulze, Phys. Lett B562 (2003) 153.
- [24] M. Baldo, G. F. Burgio, P. Castorina, S. Plumari, D. Zappalà, Phys. Rev. C75 (2007) 035804.
- [25] M. Baldo, G. F. Burgio, P. Castorina, S. Plumari, D. Zappalà, arXiv:hep-ph/0710.5388.
- [26] S. Lawley, W. Bentz, A. W. Thomas, J. Phys. G: Nucl. Part. Phys. 32 (2006) 667.
- [27] D. Blaschke, T. Klähn, R. Latowiecki, F. Sandin, J. Phys. G: Nucl. Part. Phys. 37 (2010) 094063.
- [28] O. G. Benvenuto, G. Lugones, Phys. Rev. D51 (1995) 1989.
- [29] G. Lugones, O. G. Benvenuto, Phys. Rev. D52 (1995) 1276.
- [30] Yu. A. Simonov, Nucl. Phys. B307 (1988) 512.
- [31] H. G. Dosch, Phys. Lett. B190 (1987) 177.
- [32] H. G. Dosch, Yu. A.Simonov, Phys. Lett. B205 (1988) 339.
- [33] H. G. Dosch, H. J. Pirner, Yu. A.Simonov, Phys. Lett. B349 (1995) 335.
- [34] Yu. A.Simonov, Ann. Phys. 323 (2008) 783; arXiv:hep-ph/0702266.
- [35] A. Di Giacomo, H. G. Dosch, V. I. Schevchenko, Yu. A. Simonov, Phys. Rep. 372 (2002) 319.
- [36] Yu. A.Simonov, M. A. Trusov, JETP Lett. 85 (2007) 598; arXiv:hep-ph/0703228.
- [37] Yu. A.Simonov, M. A.Trusov, Phys. Lett. B650 (2007) 36; arXiv:hep-ph/0703277.
- [38] E. V. Komarov, Yu. A.Simonov, Ann. Phys. (N. Y.) 323 (2008) 1230; arXiv:hep-ph/0707.0781.
- [39] E. V. Komarov, Yu. A.Simonov, arXiv:hep-ph/0801.2251.
- [40] F. I. M. Pereira, Nucl. Phys A860 (2011) 102; arXiv:hep-ph/1104.3352.
- [41] Yu. A. Simonov, Phys. Lett. B619 (2005) 293.
- [42] M. A. Shifman, A. I. Veinstein, V. I. Zakharov, Nucl. Phys. B417 (1979) 385.
- [43] J. I.Kapusta, Finite-Temperature Field Theory, Cambridge University Press, Cambridge, 1993.
- [44] M. Döring, S. Ejiri, O. Kaczmarek, F. Karsh, E. Laermann, E., Eur. Phys. Jour. C46 (2006)

- 179; arXiv:hep-lat/0509001.
- [45] M. Baldo, G. F. Burgio, P. Castorina, S. Plumari, D. Zappalà, Phys. Rev. D78 (2008) 063009.
- [46] G. F. Burgio, M. Baldo, P. Castorina, S. Plumari, D. Zappalà, arXiv:hep-ph/0901.1035.
- [47] O.Kaczmarek, F. Zantov, arXiv:hep-lat/0506019.
- [48] J. Sandweiss, RHIC News, http://www.bnl.gov/rhic/news/110607/story1.asp.
- [49] B. I. Abelev et al. (STAR Collaboration), Phys. Rev. C76 (2007) 011901; arXiv:nuc-exp/0511047.
- [50] M. Bleicher, F. M. Liu, J. Aichelin, H. J. Dressler, S. Ostapchenko, T. Piereog, K. Werner, Phys. Rev. Lett. 92 (2004) 072301; arXiv:hep-ph/0506019.
- [51] M. Baldo, P. Castorina, D. Zappalà, Nuclear Physics A 743 (2004) 3.

FIGURE CAPTION

- Fig. 1 Contours of constant E/A of strange quark matter at zero temperature and pressure for two different choices of the parameter V_1 (E/A and V_1 in GeV units). The vertical dashed line is where the energy per baryon number of the two-flavor quark matter exceeds the one of $^{56}F_{\rm e}$. Panels (a) and (c): strange quark mass as function of $\Delta\varepsilon_{\rm vac}$. Panels (b) and (d): strange quark mass as function of G_2 . The contours labeled (N) stand for the nucleon mass. The 0.93 contours correspond to 930.4 MeV energy per nucleon of $^{56}F_{\rm e}$.
- Fig. 2 Panel (a): The strangeness per baryon as function of the strange-quark mass for different choices of V_1 . Panel (b): As in panel (a), but for the baryon number density. Panel (c): As in panel (b), but for the hadronic electric charge per baryon.
- Fig. 3 Panel (a): Stability windows of SQM at zero temperature and pressure, bounded by the E/A = 0.93 GeV contour of $^{56}F_{\rm e}$ and its vertical line, for different choices of V_1 (in GeV units) labeling each contour. Panel (b): for each value of V_1 in panel (a), the respective locations of the E/A contour (solid) and its vertical line (dashed) on the horizontal axis. Panel (c): Baryon number densities at the energy per baryon of $^{56}F_{\rm e}$ as function of the strange quark mass for different values of V_1 . For $V_1 = 0.09$ GeV and $V_1 = 0.167$ GeV, we have $n_A = n_0$ at $m_s \sim 0.3$ GeV and $m_s = 0$, respectively, where $n_0 = 0.153$ fm⁻³ is the nuclear saturation number density.
- Fig. 4 Panel (a): Strangeness per baryon as function of the strange-quark mass for the given values of V_1 (in GeV units), all at E/A = 0.9304 GeV of $^{56}F_{\rm e}$. Panel (b): As in panel (a), but for the hadronic electric charge per baryon.
- Fig. 5 Panel (a): Strangeness per baryon as function of the strange-quark mass for the given nonzero u and d quark masses, V_1 and E/A (all in GeV units). The energy per baryon E/A = 0.899 GeV was taken for the purpose of comparison with the results in [4]. Panel (b): As in panel (a), but for the hadronic electric charge per baryon.

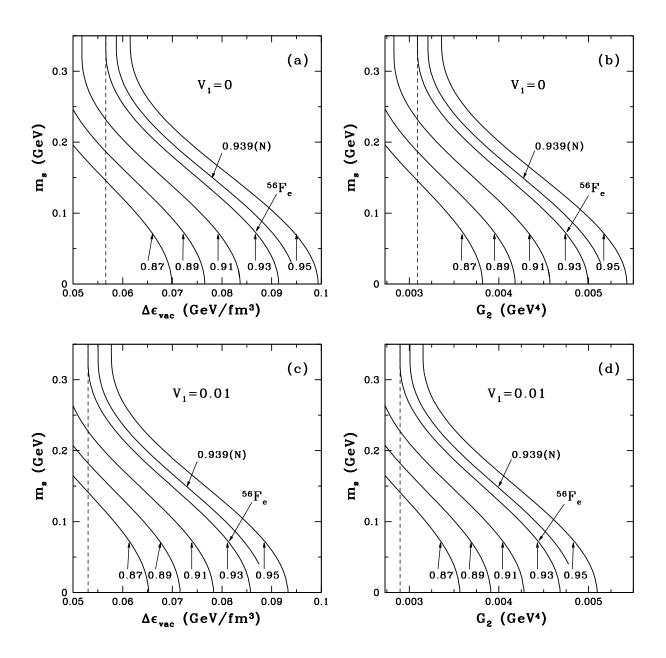


FIG. 1:

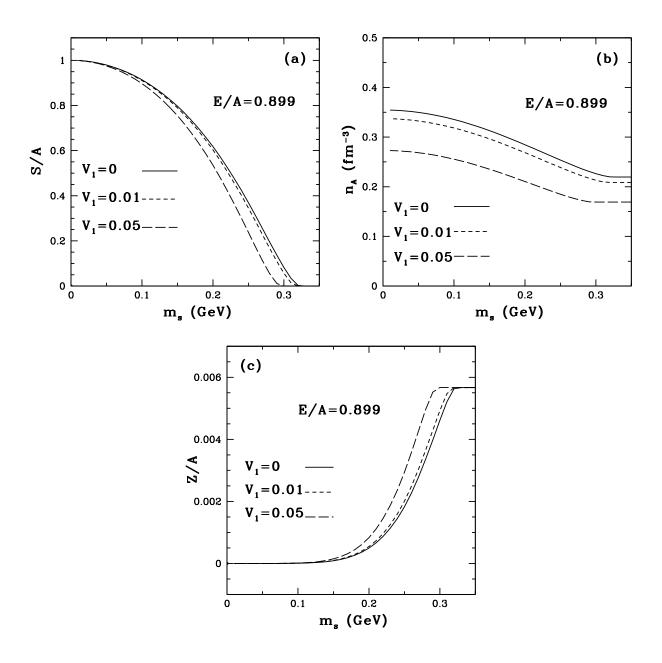


FIG. 2:

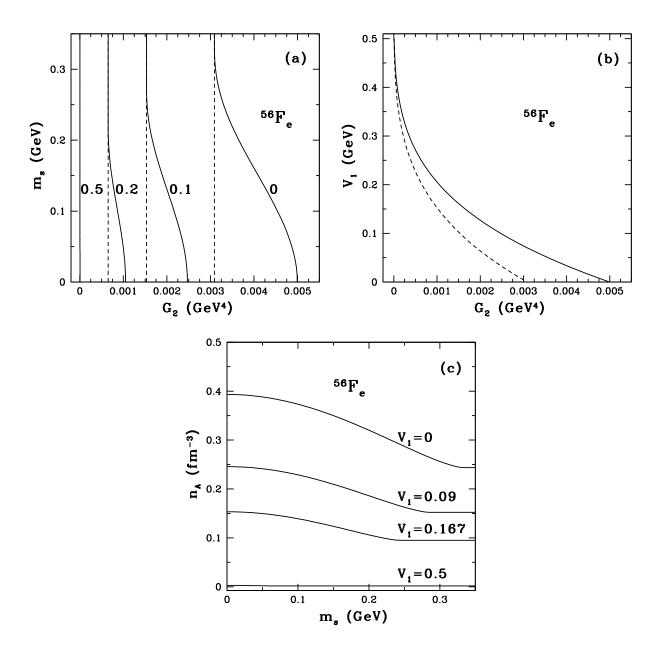


FIG. 3:

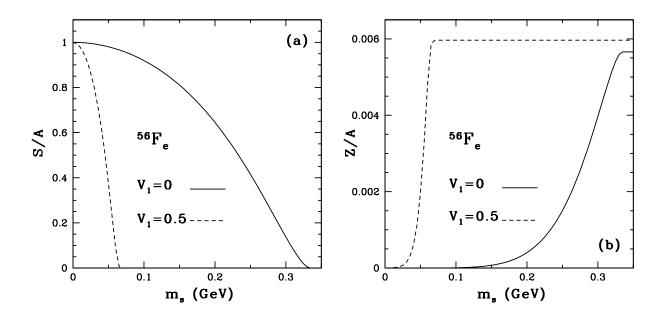


FIG. 4:

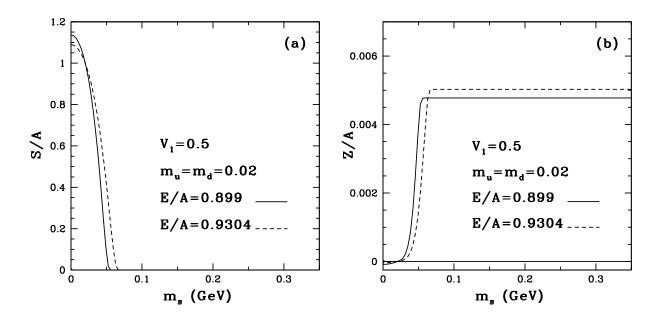


FIG. 5: